A Hybrid Finite Element Method for Conductors with Thin Dense Coatings

William E. Boyse
Andrew A. Seidl
Lockheed Palo Alto Research Laboratory
O/91-60 B/256
3251 Hanover Street
Palo Alto, CA 94304-1191

Abstract

A hybrid method of using finite elements and boundary integral methods to compute scattering from two dimensional coated conductors is presented. Finite elements are used in and around an electrically dense coating where high sampling rates are required. Since the matrix equations they generate are sparse, they can be quickly solved. The finite element sampling rate is reduced with distance from the scatterer to a very low rate where the boundary integral method provides the exact near field radiation condition. The boundary integral generates a dense matrix which is small due to the reduced sampling. This technique is compared for accuracy and efficiency with series solutions and with method of moments.

I. Introduction

Research into hybrid finite element methods is actively pursued because of their ability to efficiently and accurately model wave propagation problems with Sommerfeld's radiation conditions at infinity. Conventional methods for using finite elements, or finite differences, for these types of problems requires that the numerical boundary be far enough from the scatterer to make approximate radiation boundary conditions accurate [1] - [2]. This introduces many additional unknowns into the problem, especially in three dimensions, making a difficult problem worse. Silvester and Hsieh [3], McDonald and Wexler [4] introduced a method of coupling the finite element method to a boundary integral equation. This provided a way of terminating the numerical grid, with a boundary integral equation which satisfies the exact near field radiation condition.

Implementations of this idea can be grouped into two categories. Those employing explicit boundary integrals on arbitrary surfaces surrounding the scatterer [3] - [8], and those making use of separable geometries, circular or spherical, to reduce the boundary

integral to an algebraic equation for the modal expansion of the exterior solution [2], [9] - [11]. The modal methods have the advantage of obviating the need for a boundary integral equation, solution of which requires procedures similar to the method of moments. An advantage of the boundary integral method is that it keeps the numerical boundary close to the scatterer, thereby minimizing the number of finite element equations.

In this paper we investigate the latter method as applied to the solution of two dimensional scattering problems where a very high sampling rate is required on the scatterer. As an example, we model perfectly conducting circular cylinders coated with a thin dense material for which accurate series solutions are available for comparison. This method uses finite elements not only on the scatterer, where very high sampling rates are required, but also in a surrounding free space annulus in which the sampling rate is allowed to decrease gradually until it reaches quite a low value on the outer boundary to which the radiation condition is applied. The finite element matrix is sparse and can be solved rapidly using banded LU decomposition with partial pivoting for stability. The boundary integral can then be applied efficiently on a smooth surface in free space where the field, too, is smooth. While the matrix representing the boundary equations is dense, its dimension is small due to the low sampling rate. We compare this method with respect to accuracy with a series solution, and with respect to efficiency with a moment method.

The format of the paper is as follows. In section II, the mathematical formulation of the scattering problem and derivation of the weak form of the equations will be given. Section III will address the discretization of the finite element and boundary integral equations. Practical considerations and efficiency are discussed in section IV. Finally, numerical procedures and examples are presented in sections V and VI.

II. Analytical Foundations

Mathematical Formulation

The geometry for the two dimensional electromagnetic scattering problem considered here is depicted in Fig. 1. The region inside Γ_1 is a perfect electrical conductor while the region between Γ_2 and Γ_1 contains a smoothly varying inhomogeneous isotropic material. The region exterior to Γ_2 is free space. The formulation of the scattering problem requires that Maxwell's equations be satisfied inside Γ_3 and that the scattered field radiates to infinity. The radiation condition takes the form of of a boundary integral equation relating total and incident field points on Γ and Γ_3.

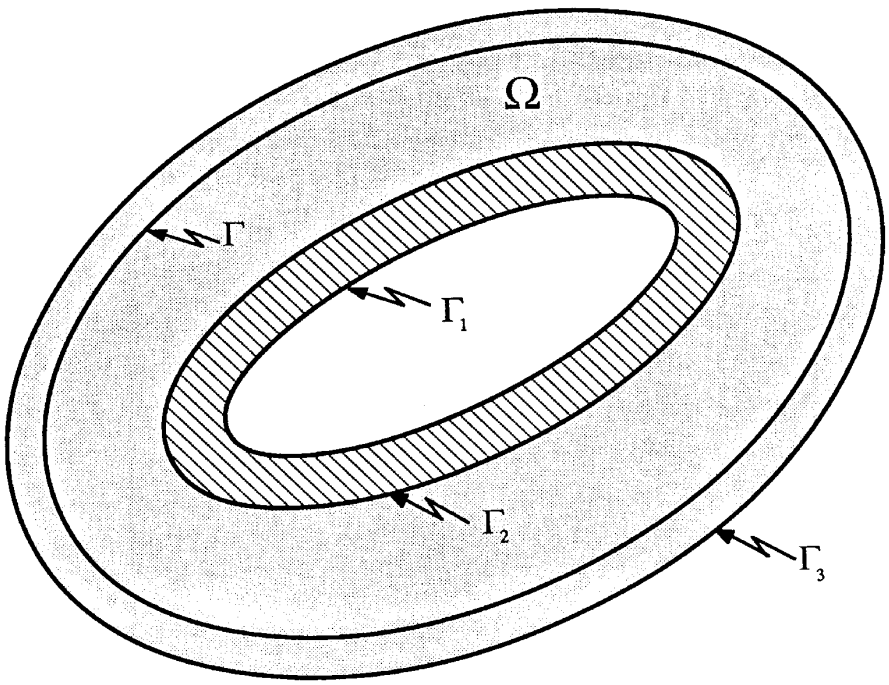

Figure 1. Geometry for hybrid finite/boundary element formulation.

We formulate both TE and TM polarized configurations in terms of a generic longitudinal field $\mathbf{F}$, which represents the magnetic field for the TE case and the electric field for TM. Thus $\mathbf{F}$ has the form $\mathbf{F} = f(x,y)\ \hat{z}$, where $\hat{z}$ is the unit vector in the z direction, and satisfies the wave equation

$$\nabla \times \alpha(x,y)\ \nabla \times \mathbf{F} - k_0^2\ \beta(x,y)\ \mathbf{F} = 0\ , \tag{1}$$

wherever α and β are smooth.
For TE we have

$$\begin{aligned} \mathbf{F} &\sim \text{ magnetic field,} \\ \alpha(x,y) &= \epsilon_0/\epsilon(x,y), \\ \beta(x,y) &= \mu(x,y)/\mu_0, \text{ and} \\ \hat{n} \times \nabla \times \mathbf{F} &= 0 \text{ on } \Gamma_1, \end{aligned} \tag{2}$$

while for TM,

$$\begin{aligned} \mathbf{F} &\sim \text{ electric field,} \\ \alpha(x,y) &= \mu_0/\mu(x,y), \\ \beta(x,y) &= \epsilon(x,y)/\epsilon_0, \text{ and} \\ \mathbf{F} &= 0 \text{ on } \Gamma_1 \end{aligned} \tag{3}$$

Here a time dependence of $e^{-\imath\omega t}$ is assumed, $k_0^2 = \omega^2\epsilon_0\mu_0$, and $\hat{n}$ is a unit normal to the surface. On the material interface, Γ_2, where α and β are discontinuous, we require that

$$(\mathbf{F}_+ - \mathbf{F}_-) = 0 \text{ and} \tag{4a}$$

$$\hat{n} \times (\alpha_+ \nabla \times \mathbf{F}_+ - \alpha_- \nabla \times \mathbf{F}_-) = 0. \tag{4b}$$

where α_+, $\mathbf{F}_+$, α_- and $\mathbf{F}_-$ denote quantities on either side of the interface. This states that the tangential components of the electric and magnetic fields are continuous across the material interface.

To specify the scattering problem we express the field on Γ_3 in terms of the incident field and the Kirchoff integral of the field on Γ.

$$\mathbf{F}(r) = \mathbf{F}^i(r) + \int_\Gamma \Big((\hat{n} \times \nabla \times \mathbf{F}(r')) G(\|r - r'\|) + (\hat{n} \times \mathbf{F}) \times \nabla G(\|r - r'\|) \Big) ds, \tag{5}$$

where $r = (x, y)$ is on Γ_3, $\mathbf{F}^i$ is the incident field, $\hat{n}$ is the outward unit normal to Γ, and $G(\|r\|) = \frac{\imath}{4} H_0^1(k_0\|r\|)$, the zeroeth order Hankel function of the first kind.

Weak Form

Formulation of the weak statement of the above problem, following Hughes [12], requires the weak form of (1) and two sets of functions, the solution space $\mathbf{S}$ and the test function space $\mathbf{V}$. The weak form is found by multiplying (1) by a test function ϕ and integrating by parts over Ω while neglecting any boundary terms. This transfers one spatial derivative from the field to the test function. The function spaces, $\mathbf{S}$ and $\mathbf{V}$, are chosen to make the weak equation well defined and to satisfy boundary conditions. We now derive the weak form of (1), show that under certain assumptions the weak solution is also a strong solution, determine the function spaces $\mathbf{S}$ and $\mathbf{V}$ to satisfy the boundary conditions and apply the radiation condition.

The weak statement of the problem is: $\mathbf{F}$ is a weak solution of (1) if f is in $\mathbf{S}$ and

$$\int_\Omega (\nabla\phi \times \alpha \nabla \times \mathbf{F} + k_0^2 \ \beta\phi\mathbf{F}) dx dy = 0, \text{ for all } \phi \text{ in } \mathbf{V} \tag{6}$$

where Ω is the region between Γ_1 and Γ_3 in Fig. 1. For our purposes, we chose functions in $\mathbf{S}$ and $\mathbf{V}$ which are continuous with piecewise continuous bounded derivatives. Therefore (4a) is satisfied by construction. The weak formulation allows one to approximate the solution of a second order differential equation by functions having only one derivative.

If $\mathbf{F}$ is a solution of (6), we assume that $\mathbf{F}$ is continuous and has continuous first and second derivatives except at discontinuities of α or β. Therefore, integrating (6) by parts

again, we obtain

$$
\begin{aligned}
-\int_{\Omega}(\nabla\phi\times\alpha\nabla\times\mathbf{F}+k_0^2\ \beta\phi\mathbf{F})dxdy &= 0 \\
&= \int_{\Omega}\phi(\nabla\times\alpha\nabla\times\mathbf{F}-k_0^2\beta\mathbf{F})dxdy \\
&+ \int_{\Gamma_1}\phi(\hat{n}\times\ \alpha\ \nabla\times\mathbf{F})\,ds \qquad (7)\\
&+ \int_{\Gamma_2}\phi(\hat{n}\times\ (\alpha_+\nabla\times\mathbf{F}_+-\alpha_-\nabla\times\mathbf{F}_-))\,ds \\
&+ \int_{\Gamma_3}\phi(\hat{n}\times\ \alpha\ \nabla\times\mathbf{F})\,ds
\end{aligned}
$$

To see that $\mathbf{F}$ is indeed a solution of the strong form of (1), consider a point in Ω not on Γ_1, Γ_2 or Γ_3. Choose the test function ϕ to be non zero in a small neighborhood of this point, and in particular $\phi = 0$ on Γ_1, Γ_2 and Γ_3. The surface integrals on the right hand side of (7) vanish since ϕ vanishes there. Since the integral over Ω must vanish for any ϕ meeting these requirements, we must have that $\nabla\times\alpha\ \nabla\times\mathbf{F}+k_0^2\beta\mathbf{F}=0$ at the chosen point. Therefore (1) is satisfied at all points of continuity of α and β, and $\mathbf{F}$ is a strong solution of (1). As a consequence of this, the integral over Ω is identically zero since the integrand vanishes pointwise. This is a standard argument in finite element analysis and can be made very precise [12], but the details will not be presented here.

In a similar manner, one can show [12] that the integrands of the three surface integrals in (7) must also vanish. From the integral over Γ_1, we see that either ϕ must vanish or $\hat{n}\times\alpha\nabla\times\mathbf{F}=0$. The latter case is called the natural boundary condition at this surface, and corresponds to a perfect electric conductor for TE, (2), and a perfect magnetic conductor for TM. The boundary condition for a perfect electric conductor must be specifically enforced in the TM case, and is called an essential boundary condition. To accomplish this, we require that for ϕ in $\mathbf{V}$ that $\phi=0$ on Γ_1, thereby obviating the natural boundary condition requirement and require that for f in $\mathbf{S}$ that $f=0$ on Γ_1, enforcing the essential boundary condition. The natural boundary condition on Γ_2 is the continuity of the tangential components of the dual field, (4b), and is satisfied automatically. The desired boundary condition on Γ_3 is the radiation boundary condition as specified by the integral (5), and is essential. Therefore we must require in both TE and TM polarizations that $\phi=0$ on Γ_3, and explicitly require that (5) is satisfied there.

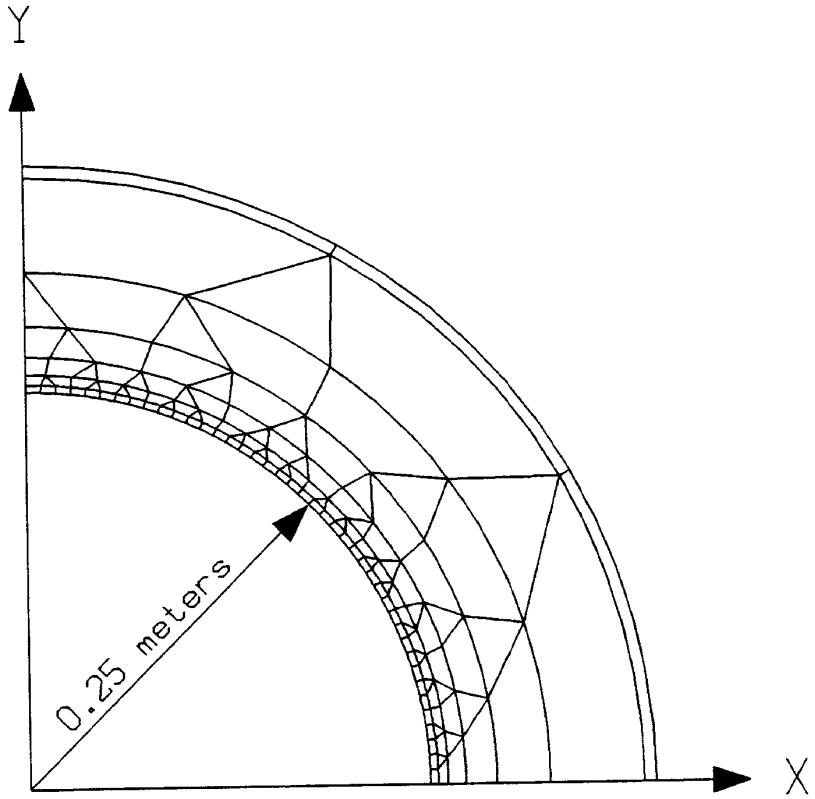

Figure 2. Finite element mesh. Coating thickness = 4.67mm.

III. Discretization

To discretize the problem the region Ω is divided into finite elements with nodes. Fig. 2 shows one quadrant of the mesh used in the examples presented in section IV. This mesh is made up of a combination of isoparametric bi-quadratic quadrilaterals and triangles, except for the outermost layer of elements where the boundary integral equation is applied. This layer of elements is quadratic in the angular direction but only linear radially. Associated with each node a is a basis function $\mathbf{N}_a(x, y)$ which equals one at the location of node a and zero at every other node, making it interpolational, and non-zero only within elements containing node a. The same basis functions are used to approximate functions in both $\mathbf{S}$ and $\mathbf{V}$ (the Galerkin approximation). We define the node sets $\mathbf{S}'$ and $\mathbf{V}'$ to be those nodes whose basis functions are used in approximating the spaces $\mathbf{S}$ and $\mathbf{V}$, respectively. Then, for TE we have

$$\begin{aligned} \mathbf{S}' &= \{ \text{ all nodes } \} \\ \mathbf{V}' &= \{ \text{ nodes not on } \Gamma_3 \}, \end{aligned} \tag{8}$$

and for TM,

$$\begin{aligned} \mathbf{S}' &= \{ \text{ nodes not on } \Gamma_1 \} \\ \mathbf{V}' &= \{ \text{ nodes not on } \Gamma_1 \text{ or } \Gamma_3 \}. \end{aligned} \tag{9}$$

If N is the number of nodes in $\mathbf{S}'$ and M is the number of nodes on Γ_3, then there are N-M nodes in $\mathbf{V}'$. For f in $\mathbf{S}$ and ϕ in $\mathbf{V}$ we have

$$f(x,y) = \sum_{a \in \mathbf{S}'} f_a \mathbf{N}_a(x,y). \tag{10a}$$

$$\phi(x,y) = \sum_{a \in \mathbf{V}'} \phi_a \mathbf{N}_a(x,y). \tag{10b}$$

Substituting (10a) and (10b) into (6), we obtain

$$\sum_{j \in \mathbf{S}'} f_j \int_\Omega \left(\nabla \mathbf{N}_k \times \alpha \nabla \times \mathbf{N}_j + k_0^2 \beta \mathbf{N}_k \mathbf{N}_j \right) dxdy = 0, \text{ for all } k \text{ in } \mathbf{V}', \tag{11}$$

which is N-M equations for N unknowns. The other M equations come from the boundary integral. Substituting (10a) into (5) and demanding equality for nodes on Γ_3, i.e. point testing, we obtain

$$f_k - \sum_{j \in \mathbf{S}'} f_j \int_\Gamma \Big((\hat{n} \times \nabla \times \mathbf{N}_j) G + (\hat{n} \times N_j) \times \nabla G \Big) ds = f_k^i, \tag{12}$$

for all nodes k on Γ_3, where f_k^i is the incident field at node k and $\hat{n}$ is the outward pointing unit normal to Γ.

IV. Practical Considerations

As mentioned in section I, an advantage of coupling finite elements to a boundary integral equation is that the numerical boundary of the problem may be placed close to the scatterer, minimizing the number of finite element equations. This, however, is not always the most efficient method. Figure 2 represents one fourth of the mesh used in subsequent numerical examples. The conducting core of radius 0.25 meters is coated with a electrically dense material occupying the first layer of elements. Here, the sampling rate must be quite high. If the boundary integral equation were applied just outside this layer, as is done in [7], the dense matrix representing this equation would be extremely large due to the high sampling rate and would dominate the numerical calculation. We increase the efficiency of this method by adding more finite elements between the scatterer and the boundary integral while decreasing the sampling rate to quite low levels.

Away from the scatterer, outside the evanescent field, the wave fields are quite smooth. This suggests that very low sampling rates may be used. We have found that six samples per wavelength, using quadratic basis functions, provides highly accurate representations. It is therefore desirable to apply the boundary integral equation in this regime where the low sampling rates translate into a system matrix of minimal dimension. In our examples,

the boundary integral equation is implemented within the outermost layer of elements. These elements are quadratic in the angular direction but only linear radially. Since the boundary integral couples all nodes in this layer of elements, reducing the radial variation to linear from quadratic reduces the number of nodes in this dense equation by one third. The shape of these elements is determined by two competing criteria. By making them thinner radially one increases the sampling rate thereby making the linear representation as accurate as the quadratic representation used angularly. If the elements are too thin, however, the distortion of the elements increases the condition number of the system. The elements used in the examples below have a radial sampling rate eight times the angular rate and provide a good compromise. In addition, the integration surface for the boundary integral, Γ in Fig. 1, passes through the center of these elements, where the derivatives are most accurate. Given this efficient and accurate representation of the near field, it is still advantageous to keep the numerical boundary close to the scatterer.

The optimal distance of the boundary integral from the scatterer is also determined by competing criteria. First, the high spatial frequencies of the evanescent field near the scatterer must be represented in detail until they have decayed below the inherent error of the discretization. This suggests a slow smooth transition from the high sampling rates near the body to the low sampling rate used in the boundary integral. A rapid transition from high to low sampling rates keeps the boundary integral close, thereby minimizing the number of finite element equations, but also highly distorts the elements, making the representation inaccurate and increasing the condition number of the system. The meshes used in the examples were generated in layers, using about a two to one reduction in the number of nodes in each subsequent layer. This reduces the sampling rate rapidly, minimizing the number of finite element equations, and does not highly distort the elements.

The efficiency gained using this method is due to the sparseness of the finite element equations. The use of finite elements to reduce the sampling rate from the quite high rate required on the scatterer to a quite low rate where the boundary integral is implemented drastically reduces the dimension of the dense boundary integral matrix at the cost of introducing additional finite element unknowns. Although the total rank of the system has been increased from what it would have been had the boundary integral been applied near the scatterer these additional finite elements generate a sparse system matrix which may be eliminated rapidly using sparse matrix algorithms. The additional time required for this extra elimination step is more than offset by the savings in reducing the dimension of the boundary integral matrix.

the boundary integral equation is implemented within the outermost layer of elements. These elements are quadratic in the angular direction but only linear radially. Since the boundary integral couples all nodes in this layer of elements, reducing the radial variation to linear from quadratic reduces the number of nodes in this dense equation by one third. The shape of these elements is determined by two competing criteria. By making them thinner radially one increases the sampling rate thereby making the linear representation as accurate as the quadratic representation used angularly. If the elements are too thin, however, the distortion of the elements increases the condition number of the system. The elements used in the examples below have a radial sampling rate eight times the angular rate and provide a good compromise. In addition, the integration surface for the boundary integral, Γ in Fig. 1, passes through the center of these elements, where the derivatives are most accurate. Given this efficient and accurate representation of the near field, it is still advantageous to keep the numerical boundary close to the scatterer.

The optimal distance of the boundary integral from the scatterer is also determined by competing criteria. First, the high spatial frequencies of the evanescent field near the scatterer must be represented in detail until they have decayed below the inherent error of the discretization. This suggests a slow smooth transition from the high sampling rates near the body to the low sampling rate used in the boundary integral. A rapid transition from high to low sampling rates keeps the boundary integral close, thereby minimizing the number of finite element equations, but also highly distorts the elements, making the representation inaccurate and increasing the condition number of the system. The meshes used in the examples were generated in layers, using about a two to one reduction in the number of nodes in each subsequent layer. This reduces the sampling rate rapidly, minimizing the number of finite element equations, and does not highly distort the elements.

The efficiency gained using this method is due to the sparseness of the finite element equations. The use of finite elements to reduce the sampling rate from the quite high rate required on the scatterer to a quite low rate where the boundary integral is implemented drastically reduces the dimension of the dense boundary integral matrix at the cost of introducing additional finite element unknowns. Although the total rank of the system has been increased from what it would have been had the boundary integral been applied near the scatterer these additional finite elements generate a sparse system matrix which may be eliminated rapidly using sparse matrix algorithms. The additional time required for this extra elimination step is more than offset by the savings in reducing the dimension of the boundary integral matrix.

V. Numerical Procedures

Efficient and accurate solution of this system of equations requires that advantage be taken of the sparsity of the system and that pivoting be used in the matrix factorization algorithm. Up to this point, the finite element development is completely analogous to that used in structural mechanics, where the method was developed and widely used [12]. However, the matrices generated in structural systems are typically real, symmetric and positive definite. The importance of positive definiteness cannot be overemphasized for it allows elimination algorithms for direct solvers to avoid pivoting [14]. For positive definite systems, the nodes may be ordered solely to minimize the computational burden. The matrix encountered here is indefinite and elimination methods must pivot for numerical stability. We address the sparsity and pivoting issues using substructuring and the LINPACK banded LU factorization algorithm [15].

The total mesh for the examples, one fourth of which is shown in Fig. 2, is in the form of an annulus. We group the nodes into two substructures. Substructure 2 contains all nodes involved in the boundary integral equation, the outermost layer of elements, and the nodes along one radial line. The remainder of the nodes are grouped into substructure 1, which after the removal of the radial line, is in the form of a strip. By numbering the nodes in this strip first across the strip, then down its length, the non-zero elements of the system matrix may be isolated into a band about the diagonal. This makes banded LU factorization, with pivoting, an appropriate algorithm.

The structure of this system of equations then becomes

$$\begin{pmatrix} K & C \\ C^T & Z \end{pmatrix} \begin{pmatrix} f_1 \\ f_2 \end{pmatrix} = \begin{pmatrix} 0 \\ f^i \end{pmatrix}, \tag{13}$$

where K is the interaction matrix for substructure 1 and is sparse and banded, Z is the interaction matrix for substructure 2 and has a large dense component, C is the coupling matrix and is sparse, C^T is the transpose of C, f_1 and f_2 are the unknowns corresponding to the two substructures and f^i is the incident field. The solution is given by

$$f_2 = \left(Z - C^T K^{-1} C\right)^{-1} f^i, \tag{14a}$$

$$f_1 = -K^{-1} C f_2, \tag{14b}$$

where $K^{-1}C$ is computed using the banded LU algorithm. The solution of (14a) is sufficient in order to compute the cross section for all illumination angles since the incident field couples only to substructure 2 and the cross section may be computed from the far field limit of (9). Solving (14b) produces the internal field.

VI. Numerical Examples

We wish to model a scatterer which requires a high sampling rate for accurate solution. To this end, we choose a conducting circular cylinder coated with a thin dense material. The parameters used for the material are the measured values of Emmerson & Cummings NZ-51, a magnetic ferrite tile. The illuminating frequency is 500 MHz, at which NZ-51 is described electrically by

$$\frac{\epsilon}{\epsilon_0} = 12.06 + \imath 0.25 \quad \text{and} \quad \frac{\mu}{\mu_0} = 7.77 + \imath 18.4. \tag{15}$$

The thickness of the coating on the one half meter diameter conducting cylinder is 0.00467 meters, exactly 1/10'th of a wavelength within the material and 1/128'th of a free space wavelength.

Fig. 2 shows one fourth of the mesh used in the example. The elements are isoparametric quadratic quadrilaterals and triangles, except for the outmost layer of elements used for the boundary integral. The innermost layer of elements model the coating. The sampling rate here is 20 nodes per internal wavelength radially and 10 nodes angularly. We found that 10 samples per wavelength radially, using elements with linear variation in this direction, was insufficient to achieve accurate results. The angular sampling rate of was also found to be about the minimum acceptable. At the outer surface of this coating, the sampling rate is 128 samples per free space wavelength. Between Γ_2 and Γ_3 a combination of quadrilateral and triangular elements to reduce the sampling rate from 128 to 6 samples per wavelength. For the TE polarized configuration there are a total of 2080 nodes on this mesh. The banded finite element matrix, K in (13), is of rank 2020 with a half band width of 140. The boundary element part of the system, Z, in (13), is 60 by 60.

The method of moments comparison represents the thin layer as one electric current on the surface of the conductor, and both electric and magnetic currents on the layer/air interface. The sampling rate is the same as that of the finite element 128 nodes per free space wavelength and produces a system matrix of 1000 by 1000. The factorization times for the finite element problem were five minutes for K and five seconds for $Z - C^T K^{-1} C$, while 90 minutes were required for the method of moments problem, both on a Vax 11/785. Even though there are over twice as many unknowns in the hybrid finite element formulation, most of these are eliminated quickly with a sparse algorithm leaving a much smaller number involved in the dense boundary integral matrix.

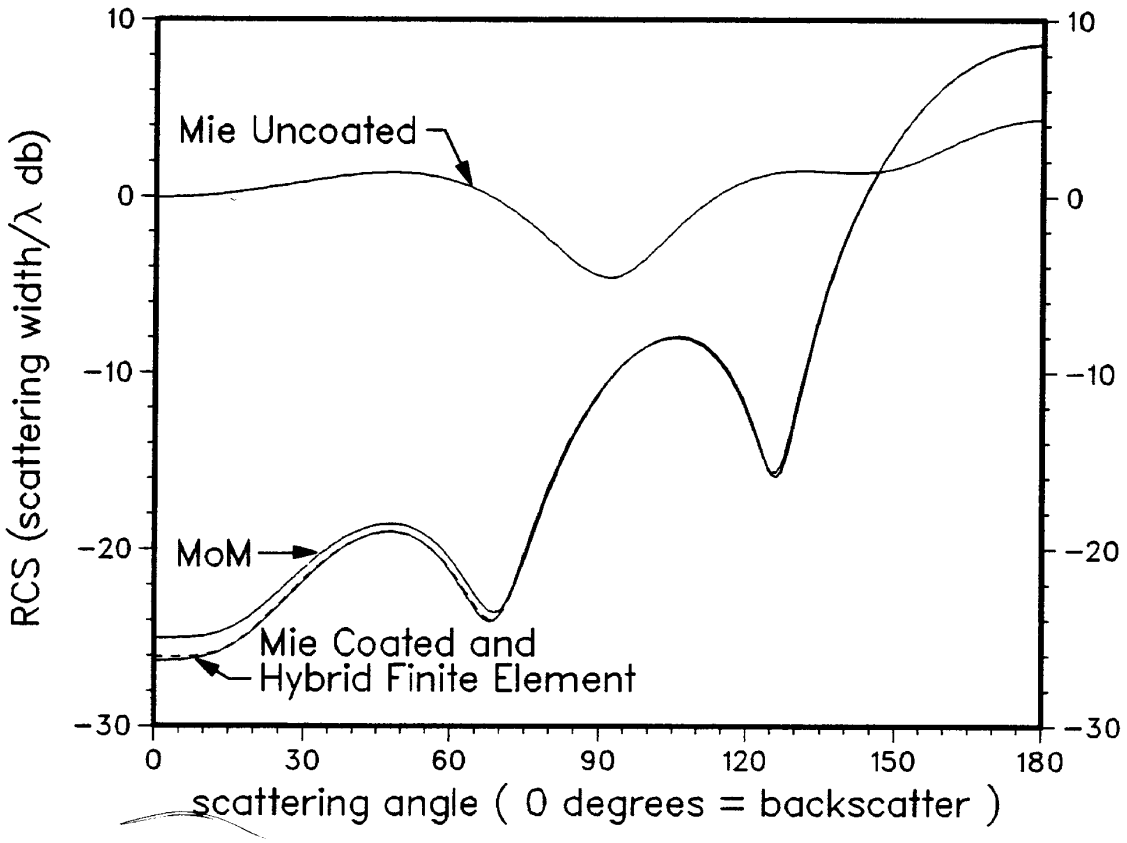

Figure 3. Bistatic scattering comparison. Coating thickness = 4.67mm.

Fig.3 shows the comparison of the bistatic cross sections for the series solution, hybrid finite element and method of moments. The upper curve, included for reference, is the series solution for the uncoated cylinder. The two bottom curves, which virtually overlie each other, are the series and hybrid finite element solutions for the coated cylinder, while the third curve from the bottom is the method of moments result for the coated cylinder. The method of moment equivalent current approach runs into difficulties with thin dense layers. This code was run at 20, 50, 100 and 128 samples per free space wavelength but was unable to equal the finite element solution in accuracy even at these extremely high sampling rates. At these high sampling rates, the hybrid finite element method is much more efficient due to the sparsity of the finite element equations and the reduced size of the dense boundary integral equations. While an impedance boundary condition is an accurate approximation to a coated perfect electric conductor, and may be implemented either with finite elements or method of moments, this hybrid finite element method is efficient and accurate where the impedance condition is inaccurate [7], and wherever high sampling rates are required for accuracy of the solution or faithful representation of the scatterer.

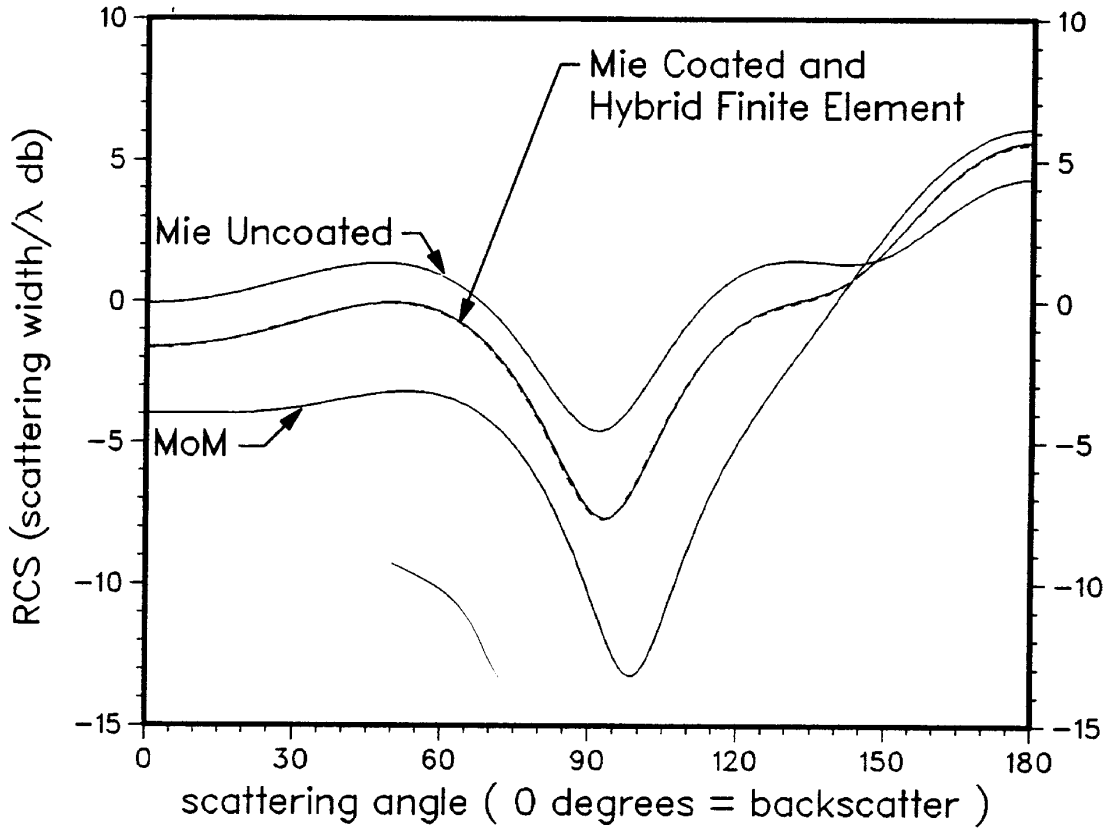

Figure 4. Bistatic scattering comparison. Coating thickness = 0.467mm.

As a second example, the same model was run except that the thickness of the coating was reduced by a factor of 10. The finite element mesh was the same as before except that the layer of elements representing the coating are too thin to be visible in the plot. The elements representing this coating were reduced to linear variation in the radial direction, providing 100 samples per interior wavelength and 1280 samples per free space wavelength. The resulting extreme variation in element sizes within the free-space annulus presented no numerical difficulty to the finite element code as Fig. 4 shows. The upper curve is again the series solution for the bare cylinder. The middle curves are the series and hybrid finite element solutions for the coated cylinder, and are virtually identical. The bottom curve is a method of moments result, at the same sampling rate as the previous example. While the moment code is experiencing great numerical difficulties in accurately representing scattering from such a thin layer, the finite element code is very accurate even in this extreme case.

It is worth noting that the TM polarized configuration is very easy in these cases, with even more accurate results, which are not shown, obtained at coarser sampling.

Conclusions

We have presented a hybrid finite/boundary element method for computing the scattering off obstacles in either TE or TM polarized configurations. This method was applied to perfectly conducting cylinders coated with thin dense materials.

We have shown that:

1) Using finite elements to move the surface where the boundary integral equation is applied some distance from the scatterer, while reducing the sampling rate, has significant computational advantages. It allows a high sampling rate to be used in and around the scattering object at a much lower cost since these "additional" unknowns are eliminated efficiently and accurately using appropriate sparse algorithms. The dimension of the dense matrix representing the boundary integral is small since this equation is applied on a smooth surface, outside of the evanescent field, where the field is smooth and thus can be sampled coarsely. For larger problems, this is even more important since the factorization time for the finite element system will grow as the circumference, while that for the boundary integral will grow as the circumference cubed, making it the dominant term in the calculation. In comparison, the method of moments equivalent current approach, or hybrid finite element methods where the boundary integral is applied very near the scatterer, generate a large dense system of equations and are much less efficient.
2) Finite elements can be used to accurately model extremely thin and dense layers. This method accurately computed the scattering from thin dense coatings which ranged from 1/128'th to 1/1280'th of a free space wavelength thick. In comparison, the method of moment equivalent current approach failed in these cases, even at extremely high sampling rates.

References

[1] A. G. Cangellaris, C. Lin and K. K. Mei, "Point-matched time domain finite element methods for electromagnetic radiation and scattering", *IEEE Trans. Antennas Propagat.*, vol. AP-35, Oct. 1987.

[2] D. Givoli and J. B. Keller, "Exact Non-reflecting Boundary Conditions", *J. Comput. Phys.*, in press.

[3] P. Silvester and M. S. Hsieh, "Finite element solution of 2-dimensional exterior field problems", *Proc. Inst. Elec. Eng.*, vol. 118, pp. 1743-1747, Dec. 1971.

[4] B. H. McDonald and A. Wexler, "Finite-element solution of unbounded field problems", *IEEE Trans. Microwave Theory Tech.*, vol. MTT-20, pp. 841-847, Dec. 1972.

[5] D. R. Lynch, K. D. Paulsen, and J. W. Strobehn, "Finite element solution of Maxwell's equations for hyperthermia treatment plannint" *J. Comput. Phys.*, vol. 58, pp. 246-269, 1985.

[6] M. V. K. Chari, J. D'Angelo, C. Crowley, J. Roeth, and H. Hurwitz, "Solution of open boundary problems by differential and integral methods", *IEEE Trans. Magnetics*, vol. MAG-22, pp. 1037-1040, Sept. 1986.

[7] J. Jin and V. V. Liepa, "Application of hybrid finite element method to electromagnetic scattering from coated cylinders", *IEEE Trans. Antennas Propagat.*, vol. 36, Jan. 1988.

[8] K. D. Paulsen, D. R. Lynch, and J. W. Strobehn, "Three-dimensional finite, boundary, and hybrid element solutions of the Maxwell equations for lossy dielectric media" *IEEE Trans. Microwave Theory Tech.*, vol. 36, pp. 682-693, 1988.

[9] K. K. Mei, "Unimoment method of solving antenna and scattering problems", *IEEE Trans. Antennas Propagat.*, vol. AP-22, pp. 760-766, Nov. 1974.

[10] M. A. Morgan and K. K. Mei, "Finite-element computation of scattering by inhomogeneous penetrable bodies of revolution", *IEEE Trans. Antennas Propagat.*, vol. AP-27, pp. 202-214, Mar. 1979.

[11] J. Lee and Z. J. Csendes, "Transfinite elements: a highly efficient procedure for modeling open field problems", *J. Applied Physics*, **61**, April 1987.

[12] T. J. R. Hughes, "The Finite Element Method - Linear Static and Dynamic Finite Element Analysis", Prentice-Hall Inc., Englewood Cliffs, New Jersey 07632.

[13] D. Colton and R. Kress (1983), *Integral Equation Methods in Scattering Theory*, John Wiley and Sons.

[14] *G. H. Golub and C. F. Van Loan (1987), Matrix Computations,* Johns Hopkins University Press, Baltimore.

[15] J. Dongarra, J. R. Bunch, C. B. Moler, and G. W. Stewart (1978), *LINPACK Users Guide*, SIAM Publications, Philadelphia.